Finite-element *Z*-matrix method: Application to electron-molecule collisions

Winifred M. Huo
NASA Ames Research Center, Moffett Field, California 94035-1000

David Brown
NASA Goddard Space Flight Center, Institute for Space Studies, New York, New York 10025

(Received 11 December 1998)

The *Z*-matrix formulation of Brown and Light [J. Chem. Phys. **101**, 3723 (1994)], based on a Kohn variational principle for a general class of finite-range scattering functionals, is applied to electron-molecule collisions employing a mixed basis of Gaussians and finite-element interpolation polynomials (times spherical harmonics). The local nature of the finite elements is particularly well suited for finite-range calculations, and all integrals involved are energy independent. The implementation of the method is designed to make use of sophisticated target functions. Numerical examples for both elastic collision of H and inelastic collision of H_2 illustrate the applicability of this approach. The results are compared with data obtained using other theoretical methods as well as experimental data. [S1050-2947(99)00407-2]

PACS number(s): 34.80.Bm, 34.80.Gs, 02.70.Dh

I. INTRODUCTION

Treatment of collision problems using space-partitioning techniques has been in practice since the introduction of the *R*-matrix method by Wigner and Eisenbud [1]. Computational efficiency is maximized by defining regions of space according to the nature of the interaction potential. For example, in electron-atom or electron-molecule collisions, the common practice is to treat the internal region, where the short-range, nonlocal nature of the electron-target interaction must be accounted for, by employing well-established methods for bound states. In the external region, the interaction potential is long range and multipolar in nature, and the collision is reduced to a one-body, potential scattering problem. Other well-established properties of space-partitioning treatments include the fact that only real matrices are involved if a real basis is used, and the *S* matrix so deduced is both unitary and symmetric.

Another advantage of these approaches is that the external region, or any regions in which the potential is local, can be subdivided into smaller sectors, and a separate *R* matrix can be constructed for each sector. The sector *R* matrices can then be assembled into a global *R* matrix for the entire region [2]. Since the computational requirements are directly proportional to the sector size, this procedure can potentially result in substantial savings in computer resources.

Both the *R* matrix and its inverse, the log derivative matrix, can be formulated using the Kohn variational principle [3–5]. Recently, Brown and Light [6] applied the Kohn variational principle to a general class of finite-range variational functionals, and derived a parametric relationship for which the functional is stationary to first-order variations in the trial wave function. This formulation, called the *Z*-matrix method, reduces to the log-derivative matrix method at a specific choice of parameters. Another choice of parameters reduces it to the *R* matrix, although it is slightly different in form from what is commonly used in the literature. Thus the *Z*-matrix formulation allows us to solve collision problems employing any of an infinite number of matrix relations depending on the choice of parameters.

Since the introduction of the *R*-matrix method to the study of *e*-atom and *e*-molecule collisions by Burke and coworkers [7,8] and by Schneider [9], it has become an important research tool in this area. The extension to include nuclear dynamics in *e*-molecule collisions was first investigated in Ref. [10]. However, up to the present most *R*-matrix studies in this area employed basis functions which obeyed a fixed boundary condition as originally formulated by Wigner and Eisenbud, instead of the fully variational formulation. The discontinuity of the wave function at the sectorial boundary is then corrected by using the Buttle correction [11]. Among earlier studies, the only *e*-molecule calculation based on the fully variational *R* matrix is the e-H_2 elastic collision study of Nesbet *et al.* [12] using an energy-dependent numerical basis. In contrast, the log-derivative matrix method, which was introduced in the fully variational form without restrictive boundary conditions [5], led to a highly efficient algorithm which is popular in the study of atom-molecule and molecule-molecule collisions. So far, neither the *Z*-matrix method nor the log-derivative matrix method has been applied to *e*-atom or *e*-molecule collisions.

The practice of employing fixed boundary conditions instead of the fully variational *R*-matrix formalism in *e*-molecule collisions is mostly related to the lack of a suitable energy-independent basis which allows flexible boundary conditions and is amenable to efficient algorithms for evaluating the necessary matrix elements with polyatomic targets. The variational calculation of Nesbet *et al.* [12] employed energy-dependent numerical asymptotic functions in their basis, so that the integrals had to be recomputed at each electron energy. This procedure eliminates one of the advantages of the *R*-matrix method, namely, that it requires the calculations of sectorial energies and eigenfunctions only once. To take advantage of energy-independent matrix elements, the numerical basis used in the UK molecular *R*-matrix package [13] are chosen to satisfy fixed boundary conditions. Another approach is to use a Gaussian basis to represent the continuum electron in the first region. The

Gaussian basis was employed in the early calculations by Schneider and co-workers [9,10], the more recent selected state *R*-matrix approach [14] as well as the UK *R* matrix for polyatomic molecules [15]. A Gaussian basis is energy independent. It also eliminates the need of imposing fixed boundary conditions. However, Gaussian basis tends to be less flexible than the piecemeal polynomials in a local basis and also more readily gives rise to linear dependency problems.

Finite elements have been successfully applied to many atomic and molecular physics problems. In particular, Shertzer and Botero [16] carried out accurate calculations of *e*-H scattering using finite elements for the radial coordinates of both electrons, thus demonstrating their utility in electron collisions. Because of their local character, finite elements are well suited for sectorial calculations. A finite element basis permits variable boundary conditions and allows full flexibility in optimizing the wave function, an important property in implementing the *Z*-matrix method. In our implementation, a mixed basis of finite elements times spherical harmonics and nuclei-centered Gaussians is used to represent the orbital of one of the electrons. The use of Gaussians provides an efficient representation of the multicentered nature of a molecular problem where the subregions at and near the nuclei require careful treatment, a result of the nuclear cusps and the high charge density there. Without using Gaussians, a large number of elements and high angular momentum functions would be required to represent the scattering electron near the nuclei. So far as we know, this is the first collision calculation using mixed local and global functions. In the first sector, we solve the $(N+1)$-electron problem. Since most accurate molecular wave functions determined by current quantum chemistry codes are expressed in terms of a Gaussian basis, we have developed an efficient algorithm to evaluate the Hamiltonian matrix element between Gaussians and finite elements. All matrix elements involved are energy independent, another attractive aspect of a finite element basis. The present approach is different from the work of Ref. [17] who reduced the *e*-molecule collision problem to a one-body potential scattering problem and computed the *R*-matrix using finite elements. Similarly, the two-dimensional finite-element calculation of Ref. [18] for electron scattering from a model H_2 potential solves an one-electron, not $(N+1)$-electron problem.

Section II presents the working equations of the *Z*-matrix method, and summarizes some relevant properties of finite elements. The implementation is discussed in Sec. III, and numerical examples are presented in Sec. IV. Section V discusses our results.

II. THEORY

A. *Z*-matrix method

Let the wave function of the $(N+1)$-electron system be $\Psi(\tau_1,\tau_2,\ldots,\tau_{N+1};\mathbf{R})$ where the electronic coordinate τ is the product of the spatial coordinate $\mathbf{r}$ and spin coordinate σ, and $\mathbf{R}$ represents the totality of the nuclear coordinates. In this paper we neglect nuclear motion. The nuclei are assumed to be in a fixed configuration $\mathbf{R}_o$ which will not be written out explicitly. The Schrödinger equations for the system are

$$(H-E)\Psi(\tau)=0, \tag{2.1}$$

$$H=H_{\rm mol}-\frac{1}{2}\nabla^2_{\mathbf{r}_{N+1}}+\sum_{i=1}^{N}\frac{1}{|\mathbf{r}_{N+1}-\mathbf{r}_i|}-\sum_{k=1}^{M}\frac{Z_k}{|\mathbf{r}_{N+1}-\mathbf{R}_k|},$$

$$H_{\rm mol}=-\frac{1}{2}\sum_{i=1}^{N}\nabla^2_{r_i}+\sum_{i>j=1}^{N}\frac{1}{|\mathbf{r}_i-\mathbf{r}_j|}-\sum_{i=1}^{N}\sum_{k=1}^{M}\frac{Z_k}{|\mathbf{r}_i-\mathbf{R}_k|}+\sum_{k>l=1}^{M}\frac{Z_kZ_l}{|\mathbf{R}_k-\mathbf{R}_l|}. \tag{2.2}$$

Here the label $N+1$ denotes the continuum electron. Due to the indistinguishability of electrons, this labeling is purely arbitrary. Also, atomic units are used throughout.

Equation (2.1) is solved using space-partitioning techniques, to be described briefly below. The present treatment differs slightly from that of Brown and Light [6], but the working equations are essentially the same. It is assumed that only one of the $N+1$ electrons, the incident or scattered electron, will be found at infinite distances from the center of mass of the molecule. As in the *R*-matrix treatment of electron collisions, the first sector is chosen such that all short-range, nonlocal interactions between the scattering electron and target are negligibly small outside its boundary. Let

$$\psi_{mn}(r_{N+1})=\int d\tau_1\cdots d\tau_N d\hat{r}_{N+1}d\sigma_{N+1}\xi^{\dagger}_m(\tau_1,\ldots,\tau_N,\hat{\mathbf{r}}_{N+1},\sigma_{N+1})\Psi_n(\tau_1,\ldots,\tau_N,\tau_{N+1}). \tag{2.3}$$

The indices *m* and *n* are *collective* indices comprising all electronic, angular momentum, and spin quantum numbers needed to describe the system at fixed r_{N+1}. The spin-space functions ξ_m form a complete set on the hypersurface of constant r_{N+1}. Typically ξ_m is expressed by a product of target eigenfunctions, spherical harmonics in $\hat{\mathbf{r}}_{N+1}$, and spin functions for the scattering electron. Ψ_n is a scattering eigenfunction whose only incoming wave component at large r_{N+1} is associated with ξ_n.

At the boundary between sectors, defined as a hypersurface of $r_{N+1}=s$, the trial function $\tilde{\Psi}_n$ and its variation $\delta\tilde{\Psi}_n$ are defined by the boundary conditions

$$a\,\tilde{\psi}_{mn}(s)+b\,\tilde{\psi}'_{mn}(s)=c_{mn},$$
$$a\,\delta\tilde{\psi}_{mn}(s)+b\,\delta\tilde{\psi}'_{mn}(s)=0, \tag{2.4}$$

where $\tilde{\psi}'_{mn}(s)$ is the outer normal derivative of $\tilde{\psi}_{mn}(s)$. Note that the matrix $\mathbf{c}$ with elements c_{mn} must be invertible.

Note that Eq. (2.4) only requires the existence of c_{mn}. Its value is not fixed *a priori*. Consider the functional

$$i_{mn}=\langle\tilde{\Psi}_m|H-E|\tilde{\Psi}_n\rangle, \tag{2.5}$$

with the inner product evaluated over the entire range of all variables except r_{N+1}, the latter covering only the range $(0,s)$. Obviously, it is nonstationary with respect to variations in $\tilde{\psi}$. However, it can be shown [6] that a related functional

$$I_{mn}=[\mathbf{c}^{\dagger}Z\mathbf{c}]_{mn}=-\left\{2i_{mn}+\sum_p\ (a\ \tilde{\psi}_{pm}+b\ \tilde{\psi}'_{pm})\times(d\ \tilde{\psi}_{pn}+e\ \tilde{\psi}'_{pn})\right\} \tag{2.6}$$

is stationary with respect to first-order variations in $\tilde{\Psi}$ if the parameters a,b,d, and e satisfy the relationship

$$ae-bd=-1. \tag{2.7}$$

Strictly speaking, the summation in Eq. (2.6) should go to infinity. In practice, of course, only enough surface states to describe the wave functions at $r_{N+1}=s$ need be included. In addition, in order for $\mathbf{c}$ to be invertible, states with incoming wave components in closed channels need to be defined even though they are not labeled explicitly in the formalism.

When the functions $\tilde{\Psi}$ are the exact eigenfunctions subject to the boundary conditions Eq. (2.4), the Z matrix obeys the equation

$$Z[a\ \Psi(s)+b\ \Psi'(s)]=d\ \Psi(s)+e\Psi'(s). \tag{2.8}$$

Here $\Psi(s)$ denotes the eigenfunction evaluated at $r_{N+1}=s$. It is easy to show that while the quantities I_{mn} depend on the specific boundary conditions $\mathbf{c}$, *the Z matrix does not*. Thus, the Z matrix computed from *any* choice of $\mathbf{c}$ will affect transformation (2.8) for any other linear combination of degenerate scattering eigenfunctions at energy E. The importance of this point will be seen below.

There is an infinite number of choices of the parameters a,b,d, and e which satisfy Eq. (2.7). Let $a=e=0$ and $b=d=1$; Eq. (2.8) is reduced to the familiar R-matrix expression

$$R\ \Psi'(s)=Z[a=e=0,b=d=1]\Psi'(s)=\Psi(s). \tag{2.9}$$

Note that the R matrix derived here has a slightly different form from other variational derivations [4]. The choice of $a=-e=1$ and $b=d=0$ reduces Eq. (2.8) to the log-derivative matrix equation, apart from a sign change

$$Y\ \Psi(s)=-Z[a=-e=1,b=d=0]\Psi(s)=\Psi'(s). \tag{2.10}$$

The log-derivative matrix obtained this way is identical with the result of Manolopoulos, D'Mello, and Wyatt [5], except for the change in sign.

1. Basis set expansion

Let the trial function $\tilde{\psi}$ be represented by a basis $\{\chi\}$. Thus Ψ for the collision system is written as

$$\Psi(\tau_1,\ldots,\tau_N,\tau_{N+1})=\sum_{mi}\ \zeta_{mi}\mathcal{A}\{\chi_i^m(r_{N+1})\xi_m(\tau_1,\ldots,\tau_N,\hat{r}_{N+1},\sigma_{N+1})\}. \tag{2.11}$$

The antisymmetrizer $\mathcal{A}$ permutes the $(N+1)$th electron with electrons $1,\ldots,N$. It is assumed that the target wave function contained in ζ_{mi} is already antisymmetrized. The requirement that the variational functional be stable with respect to first-order variations in the expansion coefficients ζ and subject to the boundary conditions in Eq. (2.4) as well as orthogonality constraints gives the following expression for the Z matrix [6],

$$Z_{mn}=-2[(U^TM_S^{-1}U)^{-1}]_{mn} \tag{2.12}$$

where

$$M_S=\tfrac{1}{2}(H-E+H^T-E^T)-\tfrac{1}{4}\sum_p\ (\mathbf{u}^p\mathbf{v}^{p^T}+\mathbf{v}^p\mathbf{u}^{p^T}) \tag{2.13}$$

with vectors $\mathbf{u}^p$ and $\mathbf{v}^p$ defined to have elements

$$u^p_{im}=(a\ \chi_i^p(s)+b\ \chi_i^{p\prime}(s))\delta_{mp},$$

$$v^p_{im}=(d\ \chi_i^p(s)+e\ \chi_i^{p\prime}(s))\delta_{mp}, \tag{2.14}$$

and the pth column of matrix U just the vector $\mathbf{u}^p$. Note that the appearance of the Kronecker deltas in Eq. (2.14) assumes that the surface functions ξ are orthogonal; if they are not, the Kronecker deltas must be replaced with the overlaps of ξ_m and ξ_p.

2. Z-matrix propagation

The propagation of the Z matrix is analogous to that of the R matrix [2]. Assume a Z matrix on $(0,\ s_1)$ has been constructed using the foregoing procedure which affects the mapping

$$Z_1[a\ \Psi(s_1)+b\ \Psi'(s_1)]=d\ \Psi(s_1)+e\Psi'(s_1). \tag{2.15}$$

Similarly we can construct on the range (s_1,s_2) a 2×2 Z matrix to perform the mapping,

$$Z_2\left[a\begin{pmatrix}\Psi(s_1)\\ \Psi(s_2)\end{pmatrix}+b\begin{pmatrix}\Psi'(s_1)\\ \Psi'(s_2)\end{pmatrix}\right]=\left[d\begin{pmatrix}\Psi(s_1)\\ \Psi(s_2)\end{pmatrix}+e\begin{pmatrix}\Psi'(s_1)\\ \Psi'(s_2)\end{pmatrix}\right]. \tag{2.16}$$

By invoking the continuity of Ψ and its derivative at s_1, $\Psi(s_1)$ and $\Psi'(s_1)$ can be eliminated, yielding an expression for the Z matrix on the range $(0,s_2)$ in terms of Z_1 and Z_2.

3. Z matrix and S matrix

The relationship between the Z matrix and the S matrix is obtained using outgoing scattering wave boundary conditions [6]. Let s_o be the distance where the wave function reaches its asymptotic form. The S matrix is given by

$$S=[Z(a\,O+b\,O')-(d\,O+e\,O')]^{-1}\times[Z(a\,I+b\,I')-(d\,I+e\,I')], \tag{2.17}$$

with the matrix elements of I and O given by

$$I_{mn}=\frac{1}{\sqrt{k_m}}e^{-ik_m s_o}\delta_{mn},\qquad O_{mn}=\frac{1}{\sqrt{k_m}}e^{ik_m s_o}\delta_{mn}, \tag{2.18}$$

where $k_m=\sqrt{2(E-\epsilon_m)}$, and ϵ_m is the mth eigenvalue of the N-electron (atomic or molecular) Hamiltonian.

Since the Z matrix has components which couple closed channels to open channels, and closed channels to one another, the S matrix defined in Eq. (2.17) shares this characteristic, as is the case with the R matrix. The open-open subblock is the physical S matrix, and is unitary as long as Z is real symmetric.

In the actual computer code, the inverse of Z is used to compute S. By inserting ZZ^{-1} between the two bracketed matrices in Eq. (2.17), the S matrix can be expressed in terms of Z^{-1} instead of Z. In this manner the matrix inversion step in the expression of Z in Eq. (2.12) can be avoided.

4. Choice of parameters

The values of the parameters $a,b,d,$ and e which reduce the Z matrix to the R matrix and log-derivative matrix are given in Eqs. (2.9) and (2.10). There are of course infinite other choices of the parameters which satisfy Eq. (2.7) and give variationally stable solutions. This flexibility offers additional advantages to the Z-matrix method over the R-matrix and log-derivative matrix methods. Calculations using different choices of parameters should converge to the same result, thus providing an internal check on basis set convergence. An example of this was given in Ref. [6], and another example will be given in Sec. IV of this paper. In addition, it is noted that the eigenvalues of $\frac{1}{2}(H+H^T)-\frac{1}{4}\Sigma_p(\mathbf{u}^p\mathbf{v}^{pT}+\mathbf{v}^p\mathbf{u}^{pT})$ in Eq. (2.12) depend on the value of the parameters. When the energy used in the calculation accidentally coincides with one of the eigenvalues, causing the inversion of the matrix M_S to fail, it is always possible to shift the eigenvalues by using a different choice of parameters. In contrast, the R matrix and log-derivative matrix calculations would require the use of a different energy.

B. Finite elements

In finite-element analysis, the coordinate space is discretized into small regions called elements [19]. For the one-dimensional case considered here, the local coordinate x, defined only inside the element, is related to the global coordinate r and the boundaries of the element r_a and r_b by

$$x=\frac{2r-(r_b+r_a)}{r_b-r_a}. \tag{2.19}$$

The value of x ranges from -1 to 1. Interpolation polynomials in terms of the local coordinates serve as a basis to represent the function of interest. By decreasing the element size, or by increasing the degree of the interpolation polynomials, it is possible to improve the accuracy of the representation systematically. In this paper, fifth degree Hermite interpolation polynomials [20] are used. Thus three nodes are assigned to each element, at the local coordinates $x=-1,0,$ and 1. Fifth degree Hermite interpolation polynomials $p_m(x)$ have the following values at nodes $n=1$–3:

$$p_m(x)=\begin{cases}1, & m=2n-1\\ 0 & \text{otherwise,}\end{cases}\qquad \frac{dp_m(x)}{dx}=\begin{cases}1, & m=2n\\ 0 & \text{otherwise.}\end{cases} \tag{2.20}$$

The continuity of the function and its derivative across element boundaries is achieved by requiring the expansion coefficients associated with the last two Hermite polynomials in an element, representing the function and its derivative at the boundary, to have the same values as those associated with the first two polynomials of the next element.

The Hermite interpolation polynomials belonging to the same element are nonorthogonal. Those of different elements naturally are orthogonal to each other, since their space do not overlap. Thus the Hamiltonian matrix represented by finite elements is a sparse matrix if the potential is local. When exchange interaction is involved, the Hamiltonian matrix is no longer sparse, but still block diagonal dominant. Due to its local nature, finite elements are well suited for sectorial calculations. For example, at the outer surface s of a sector, the vector $\mathbf{u}^p$ in Eq. (2.14), represented by finite elements, will have only two nonvanishing components; those associated with the last and next to last Hermite polynomials.

Because the Hermite polynomials form a nonorthogonal basis, when a mixed finite element and Gaussian basis is used, no attempt is made to orthogonalize these two basis sets. This choice is made because imposing the orthogonality constraint will remove the block-diagonal dominant feature of the Hamiltonian matrix represented by elements.

III. IMPLEMENTATION

The following trial function is used for the $(N+1)$-electron system,

$$\Psi(\tau)=\sum_n \mathcal{A}\{\Phi_n(\tau_1,\ldots,\tau_N)f_n(\tau_{N+1})\} + \sum_d \lambda_d\Theta_d(\tau_1,\ldots,\tau_{N+1}). \quad (3.1)$$

The fixed-nuclei target function $\Phi_n(\tau_1,\ldots,\tau_N)$ is expressed in terms of a Gaussian basis and the quality of the wave function varies from simple self-consistent field functions to large configuration-interaction functions. If the first sum in Eq. (3.1) is over the complete set of target functions including the continuum, then the second sum is unnecessary and we have a close-coupling wave function. In practice, the first sum almost always has to be truncated [21]. Thus the second sum in Eq. (3.1), consisting of $(N+1)$-electron functions Θ represented by a pure Gaussian basis, is introduced to account approximately for the role of the missing terms in the first summation. Two types of Θ are included. One is to describe the polarization and correlation effects between the target and the continuum electron, and the other is to represent the high-angular-momentum part of the continuum orbital important in the region near the nuclei. In other *ab initio* methods, Θ is also used to relax the orthogonality constraint between the bound and continuum functions. In the present case, the use of a nonorthogonal basis eliminates this need. Since both types of Θ result from short-range interactions, they are important only in the internal region. Consequently, it is sufficient to represent Θ by a Gaussian basis. It is worthwhile pointing out that finite elements can represent both bound and continuum functions, and a mixed finite-element and Gaussian basis can also be adopted to represent Θ. However, such representations are less compact. Hence a pure Gaussian basis is employed. Except for the fact that Θ is not used to relax the orthogonality constraint, its role is analogous to the ''square integrable functions'' employed in the UK *R*-matrix package [13] and the *Q*-space configurations used in the complex Kohn method [22].

The continuum electron is represented by a mixed basis consisting of Gaussians and products of finite elements and spherical harmonics. The one-electron spin orbital for the continuum electron, g_n, is given by,

$$g_n(\tau_{N+1})=f_n(\tau_{N+1})+\psi_n(\tau_{N+1}), \quad (3.2)$$

with

$$f_n(\tau_{N+1})=\frac{1}{r_{N+1}}\sum_{\alpha,i}\sum_{l,m}\zeta^{(\alpha)}_{n,ilm}\,p^{(\alpha)}_i(x)Y_{lm}(\hat{r}_{N+1})\omega(\sigma_{N+1}), \quad (3.3)$$

$$\psi_n(\tau_{N+1})=\sum_j \zeta_{n,j}\,\phi_j(\mathbf{r}_{N+1})\omega(\sigma_{N+1}). \quad (3.4)$$

Note that $f_n(\tau_{N+1})$ is associated with the first term in Eq. (3.1), whereas $\psi_n(\tau_{N+1})$ is obtained from the second term by projecting out the target wave function $\Phi_n(\tau_1,\ldots,\boldsymbol{\tau}_N)$. In the above ϕ_j is a Gaussian orbital, ω is the spin function, and Y_{lm} are real spherical harmonics. If complex spherical harmonics are used, the integral between Y_{lm} and Gaussians is complex. It has the disadvantage of doubling the storage requirements for the integrals. The interpolation polynomial $p^{(\alpha)}_i(x)$, with α labeling the element and i the polynomial in the element, is written in terms of the local coordinate x instead of the global coordinate r_{N+1}. The origin of the coordinate $\mathbf{r}_{N+1}$ for the finite element expansion is chosen to be the center of mass. The boundary condition of $f_n(\tau_{N+1})$ at $r_{N+1}=0$ requires the coefficients $\zeta^{(\alpha)}_{n,ilm}$ to satisfy the relationships

$$l=0,\quad \zeta^{(\alpha)}_{n,ilm}=0 \quad \text{if } \alpha=1,\quad i=1,$$
$$l>0,\quad \zeta^{(\alpha)}_{n,ilm}=0 \quad \text{if } \alpha=1,\quad i=1 \text{ and } 2. \quad (3.5)$$

The function ϕ_j is a one-electron function composed of nuclei-centered Gaussians. At the least, ϕ_j is obtained from a linear combination of Gaussians, so it has the correct point group symmetry of the system under study. In most cases, it comes from the set of one-electron orbitals obtained in the course of determining the target function. As in the case of target functions, it is also supposed to vanish at the boundary of the internal region. Note also that the Gaussians and the Hermite polynomials are not orthogonal to each other.

Because the interaction potential in the internal region (first sector) and the external region (*n*th sector, $n>1$) are different, the evaluation of the Hamiltonian matrix elements is also different. In the following, the two regions are discussed separately.

A. Internal region

Here the $(N+1)$-electron interaction has to be explicitly accounted for. The calculation of the Hamiltonian matrix elements, H_{ij}, in a mixed finite-element and Gaussian basis requires the integrals between hermite polynomials and Gaussians. All integrals are evaluated numerically. Two-electron integrals are done using a two-step procedure: evaluation of the potential due to the charge distribution of electron 1 by solving Poisson's equation, and numerical integration of the charge distribution of electron 2 over the potential. Except when the angular integrals are analytic, numerical integration in the angular coordinates are also done using finite elements. Details of the integral calculation are given elsewhere [23].

While the Gaussian orbitals used to represent the target functions and the closed channel space Θ form an orthogonal set, a nonorthogonal basis is used to expand the one-electron orbital for the continuum electron, resulting in a nonorthogonal representation of Ψ. Thus the overlap matrix is maintained in all calculations, and the E matrix in Eq. (2.13) is the energy E times an overlap matrix.

The evaluation of H_{ij} over a nonorthogonal basis is not in the standard quantum chemistry codes. Thus the calculation of H_{ij} is separated into two steps. The matrix elements involving pure Gaussian orbitals are evaluated using the conventional-configuration-interaction (CI) matrix generator code DVDCI in the quantum-chemistry code SWEDEN [24]. A new matrix generator code is written to handle the matrix elements involving a nonorthogonal basis, i.e., between $\mathcal{A}\Phi_i(\tau_1,\ldots,\tau_N)f_i(\tau_{N+1})$ and $\mathcal{A}\Phi_j(\tau_1,\ldots,\tau_N)f_j(\tau_{N+1})$

and between $\mathcal{A}\Phi_i(\tau_1,\ldots,\tau_N)f_i(\tau_{N+1})$ and Θ_j. Because only one orbital in the $(N+1)$-orbital function is represented by a nonorthogonal basis, the expression of H_{ij} is significantly simpler than the case when the full $N+1$ orbitals are expressed by a nonorthogonal basis. Making use of the fact that H_{ij} vanishes unless Φ_i and Φ_j differ by at most two spin orbitals, it can be expressed in terms of the two-electron (transition) spin density $D_{ij}^{(2)}(\tau_1\,\tau_2|\tau_{1'}\,\tau_{2'})$ of $\Phi_j^*\Phi_i$ [25]:

$$D_{ij}^{(2)}(\tau_1\,\tau_2|\tau_{1'}\,\tau_{2'})=\frac{N(N-1)}{2}\int d\tau_3\cdots d\tau_N\Phi_j^*(\tau_1'\tau_2'\tau_3,\ldots,\tau_N)\Phi_i(\tau_1\tau_2\tau_3,\ldots,\tau_N). \tag{3.6}$$

The two-electron spin-density matrix $P_{ij}^{(2)}(pq|p'q')$ is obtained by representing $D_{ij}^{(2)}(\tau_1\,\tau_2|\tau_{1'}\,\tau_{2'})$ in terms of a complete set of Gaussian orbitals ϕ_p,ϕ_q,

$$D_{ij}^{(2)}(\tau_1\,\tau_2|\tau_{1'}\,\tau_{2'})=\sum_{p,p'q,q'}P_{ij}^{(2)}(pq|p'q')\phi_p(\tau_1)\phi_q(\tau_2)\phi_{p'}(\tau_{1'})\phi_{q'}(\tau_{2'}). \tag{3.7}$$

In terms of $P_{ij}^{(2)}(pq|p'q')$, the expectation of a two-electron operator F is given by

$$\langle\Phi_j|F|\Phi_i\rangle=\sum_{pqp'q'}P_{ij}^{(2)}(pq|p'q')\langle\phi_p\phi_q|\hat{f}|\phi_{p'}\phi_{q'}\rangle,$$

$$F=\sum_{\mu_1<\mu_2}\hat{f}_{\mu_1\mu_2}. \tag{3.8}$$

H_{ij} can be rewritten as

$$H_{ij}=\sum_{pqp'q'}P_{ij}^{(2)}(pq|p'q')\langle\mathcal{A}_3\phi_{p'}(\tau_1)\phi_{q'}(\tau_2)f_j(\tau_{N+1})|\hat{h}|\mathcal{A}_3\phi_p(\tau_1)\phi_q(\tau_2)f_i(\tau_{N+1})\rangle. \tag{3.9}$$

Here $\mathcal{A}_3$ permutes electrons 1, 2, and $N+1$, and $\hat{h}$, analogous to $\hat{f}$, is a Hamiltonian operator for three electrons:

$$\hat{h}=\hat{h}_{\rm mol}+\frac{2}{N(N-1)}\left\{-\frac{1}{2}\nabla_{\mathbf{r}_{N+1}}^2-\sum_{k=1}^{M}\frac{Z_k}{|\mathbf{r}_{N+1}-\mathbf{R}_k|}+\frac{N}{|\mathbf{r}_{N+1}-\mathbf{r}_1|}\right\},$$

$$\hat{h}_{\rm mol}=\frac{2}{N-1}\left\{-\frac{1}{2}\nabla_{r_1}^2-\sum_{k=1}^{M}\frac{Z_k}{|\mathbf{r}_1-\mathbf{R}_k|}+\sum_{k>l=1}^{M}\frac{Z_kZ_l}{N|\mathbf{R}_k-\mathbf{R}_l|}\right\}+\frac{1}{|\mathbf{r}_1-\mathbf{r}_2|}. \tag{3.10}$$

H_{ij} between $\mathcal{A}\Phi_i(\tau_1,\ldots,\tau_N)f_i(\tau_{N+1})$, and Θ_j can also be rewritten in a similar manner. Thus the calculation of H_{ij} reduces to the evaluation of a three-electron Hamiltonian matrix element, regardless of the value of N. There are two advantages to this approach. Because the target wave function $\Phi_i(\tau_1,\ldots,\tau_N)$ is used in the generation of D_{ij}, the phase relationship is kept intact. There is no need to carry out a pseudo-$(N+1)$-electron calculation to circumvent the phase consistency problem, which can be encountered when the configuration-state-function generator in quantum-chemistry codes is directly used in electron-molecule collision calculations [26,13,27]. Also, in the future publicly distributed quantum-chemistry codes are likely to include two-electron-spin densities in the package. This approach enables us to employ the quantum chemistry calculation directly without having to handle CI wave functions with hundreds of millions of configurations.

B. External region

In the external region, the problem reduces to a one-electron, coupled-channel problem, and can be handled in a straightforward manner. A pure finite-element basis is used to represent the radial function. As in the R matrix approach, the solution of the external region is obtained by further partitioning into as many sectors as necessary, and then the Z matrices are reassembled into a global Z matrix.

IV. NUMERICAL EXAMPLES

A. *e*-H elastic scattering in the static-exchange approximation

The hydrogen-atom wave function is represented by a basis of seven Gaussians. Due to the spherical symmetry of the system, a pure finite-element basis is used to represent the continuum electron. Also, the short-range nature of the *e*-H static-exchange potential requires only three sectors to reach an asymptotic behavior. Each sector uses 24 elements. In the first sector (inner region), the element boundaries are 0, 0.1, 0.2, 0.4, 0.6, 0.8, 1, 1.25, 1.5, 1.75, 2, 2.5, 3, 4, 5, 6, 7, 8, 9, 10, 11, 12, 13, 14, and 15. At the boundary of the first sector, the most diffuse Gaussian function has a value $\approx 10^{-8}$. At the two outer sectors they are evenly spaced at 1-a.u. intervals. To test the invariance of the result using different

TABLE I. Eigenphase sum (radians) of *e*-H elastic scattering in the static-exchange approximation. ^1S channel.

Energy (a.u.)	Log derivative	*R*	*Z*1	*Z*2	Mott and Massey[a]
0.005	2.395 322 16	2.395 322 16	2.395 322 16	2.395 322 16	2.396
0.025	1.869 315 62	1.869 315 62	1.869 315 62	1.869 315 62	1.871
0.045	1.507 462 51	1.507 462 51	1.507 462 51	1.507 462 51	1.508
0.080	1.239 077 38	1.239 077 38	1.239 077 38	1.239 077 38	1.239
0.125	1.031 067 02	1.031 067 02	1.031 067 02	1.031 067 02	1.031
0.180	0.868 732 440	0.868 732 440	0.868 732 440	0.868 732 440	0.869
0.245	0.743 820 304	0.743 820 304	0.743 820 304	0.743 820 304	0.744
0.320	0.650 973 501	0.650 973 501	0.650 973 501	0.650 973 501	0.651

[a]From Ref. [28].

choices of parameter sets satisfying Eq. (2.7), the calculation was repeated using four sets of parameters: (1) $a=-e=1$ and $b=d=0$, the log-derivative matrix; (2) $b=d=1$ and $a=e=0$, the *R* matrix; (3) $a=b=1$, $d=8$, and $e=7$, designated as the *Z*1 matrix; and (4) $a=5$, $b=3$, $d=7$, and $e=4$, designated as the *Z*2 matrix. Tables I and II present the eigenphase sum computed for the ^1S and ^3S channels, respectively. Also presented are the static-exchange result tabulated in Mott and Massey [28]. For the ^1S calculations, the four sets of parameters give identical results to nine significant figures. The agreement with Mott and Massey is also good. Calculations of ^3S scattering using the same four sets of parameters agree with each other to seven significant figures except at the lowest electron energy, 0.005 a.u. In that case the agreement is only to six figures. The largest disagreement with Mott and Massey is also at the lowest energy. We believe that the difference between our result and that of Mott and Massey is mainly due to the use of a Gaussian representation for the H atom in our case instead of a hydrogenic wave function.

B. Two-channel calculation of $X\,^1\Sigma_g^+ \rightarrow b\,^3\Sigma_u^+$ of H_2 by electron impact

This example is chosen because all currently employed computational methods for *e*-molecule collisions have been used for its calculation, thus providing a good test case to compare the *Z* matrix result with other approaches. The Gaussian basis used is a $[6s3p1d|4s3p1d]$ basis with the *s* and *p* functions taken from the correlation consistent polarization valence quadruple-zeta (cc-pVQZ) basis of Dunning and co-workers [29] whereas the *d* function is taken from their cc-pVTZ basis. All calculations were done at $R=1.401\,534$ a.u. Using this basis, the ground-state CI energy equals $-1.173\,253\,68$ a.u., and the *b* state CI energy is $-0.781\,956\,00$. All CI calculations used full CI. The results are to be compared with the James-Coolidge-type correlated calculation of Kolos and Wolniewicz (KW) [30]. Interpolation of their potential-energy curves gives a ground-state energy of $-1.174\,474\,6$ and a *b*-state energy of $-0.784\,569$ at the *R* value we used. The *b*-state excitation threshold from the present calculation is 10.6478 eV versus KW's 10.6098 eV. Also, the ground-state quadrupole moment of H_2 is calculated to be 0.444 991 a.u. versus KW's value of 0.457 448 at $R=1.4$. Using this basis, the self-consistent field (SCF) energy for the ground state is $-1.133\,427\,72$, and the improved virtual orbital (IVO) energy [31] of the *b* state is $-0.765\,656\,14$. Thus the SCF excitation threshold, 10.0076 eV, is approximately 0.5 eV lower than the CI threshold. The ground-state SCF quadrupole moment is 0.484 818.

The *Z*-matrix calculation is separated into 250 sectors, with 24 elements in each sector. In the first sector (i.e., the inner region), the continuum electron is represented by both elements and Gaussians. The spherical harmonics associated with the elements are limited to $l\leqslant 6$ and $|m|\leqslant 2$. The distribution of elements in the first sector is identical with the *e*-H calculation. At the boundary of the first sector, the most diffuse Gaussian function has a value $\approx 10^{-8}$. In all remaining sectors, the elements are evenly placed at 1.0-a.u. intervals. The convergence of the calculation with respect to the number and placement of elements has been tested. It is believed that the calculated cross sections have converged to at least five significant figures.

TABLE II. Eigenphase sum (radians) of *e*-H elastic scattering in the static-exchange approximation, ^3S channel.

Energy (a.u.)	Log derivative	*R*	*Z*1	*Z*2	Mott and Massey[a]
0.005	2.905 998 49	2.905 997 49	2.905 997 54	2.905 997 83	2.908
0.025	2.677 925 46	2.677 925 29	2.677 925 37	2.677 925 38	2.679
0.045	2.460 509 66	2.460 509 52	2.460 509 44	2.460 509 53	2.461
0.080	2.256 695 12	2.256 694 89	2.256 694 97	2.256 695 00	2.257
0.125	2.069 614 04	2.069 614 04	2.069 613 98	2.069 614 02	2.070
0.180	1.900 181 42	1.900 181 24	1.900 181 24	1.900 181 29	1.901
0.245	1.748 476 84	1.748 476 84	1.748 476 84	1.748 476 85	1.749
0.320	1.613 809 27	1.613 809 17	1.613 809 10	1.613 809 17	1.614

[a]From Ref. [28].

TABLE III. Eigenphase sum (radians) of e-H_2 $X\,^1\Sigma_g^+ \rightarrow b\,^3\Sigma_u^+$ two-channel calculation, $^2\Sigma_g^+$ symmetry.

Energy (eV)	Log derivative	R	$Z1$	$Z2$
10.75	1.625 025 17	1.625 025 16	1.625 025 16	1.625 025 19
12.50	1.321 724 73	1.321 724 69	1.321 724 69	1.321 724 70
15.00	1.009 459 55	1.009 459 45	1.009 459 45	1.009 459 45
17.50	0.787 108 46	0.787 108 23	0.787 108 23	0.787 108 23
20.00	0.677 994 01	0.677 993 54	0.677 993 54	0.677 993 54
25.00	0.590 129 84	0.590 128 22	0.590 128 22	0.590 128 22
30.00	0.559 404 93	0.559 400 41	0.559 400 41	0.559 400 40

Table III presents the $^2\Sigma_g$ channel eigenphase sum at selected energies calculated using CI target functions. Here we find the results calculated using the four different parameters sets agree with each other to at least five significant figures. This is consistent with the estimated accuracy of the cross section by changing the element basis. The agreement is better at low energies, indicating that the elements chosen do not describe the high-energy part of the calculation as well. We also find that the agreement among the R matrix, $Z1$ matrix, and $Z2$ matrix is consistently better than with the log-derivative matrix. For example, at 30 eV, the agreement among the former three is to seven figures, whereas they agree with the log-derivative result only to five figures. This behavior is not fully understood at present.

Figures 1–4 compare the $X\,^1\Sigma_g^+ \rightarrow b\,^3\Sigma_u^+$ partial cross sections of $^2\Sigma_g^+$, $^2\Sigma_u^+$, $^2\Pi_{ux}$, and $^2\Pi_{gx}$ symmetries with other theoretical calculations. Because almost all previous calculations used single configuration target wave functions, the Z-matrix results presented there also were calculated using SCF target functions. To test the dependence on the Gaussian basis used, we also carried out calculation using the ccp-VDZ basis of Dunning and co-workers $[4s1p|2s1p]$. We found that the change of Gaussian basis has very little effect on the cross sections. This is consistent with the findings of Schneider and Collins [32] in their linear algebraic (LA) calculation of this system. In addition, we found the CSF's $1\sigma_g 1\sigma_u^2$ and $1\sigma_g^2 1\sigma_u$, normally used to relax the orthogonality constraints, have very little effect on the result. The cross sections with and without those terms differ at most at the third significant figure. This is a reflection of the use of a nonorthogonality basis. The need for the orthogonality relaxation terms no longer exists in our approach.

It is seen from the figures that our results are consistently in good agreement with the Schwinger multichannal (SMC) calculation of Lima *et al.* [33] and the LA calculation of Schneider and Collins, confirming the validity of the Z-matrix calculation. The agreement with the R-matrix calculation of Ref. [34] is less good, even though the R-matrix formulation is a subset of the Z-matrix method. One source

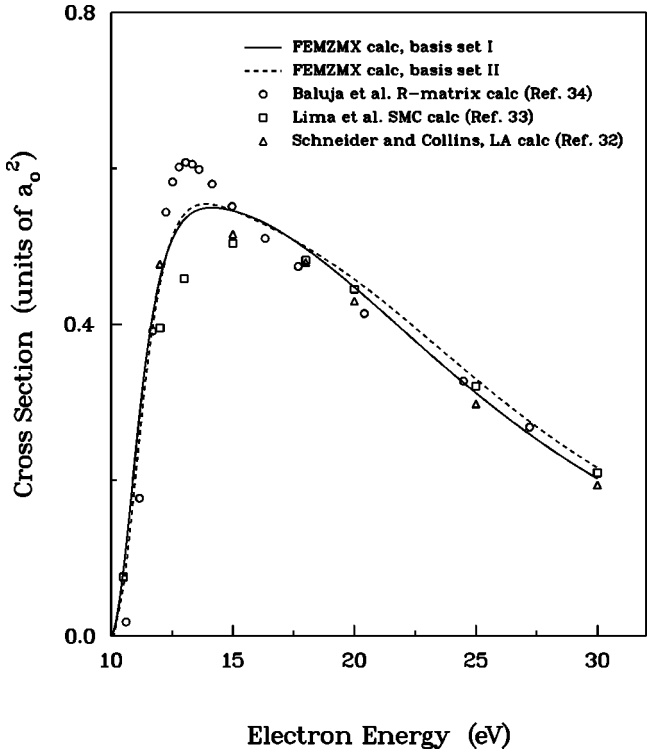

FIG. 1. Electron-impact excitation cross sections for the $X\,^1\Sigma_g^+ \rightarrow b\,^3\Sigma_u^+$ transition of H_2. $^2\Sigma_g^+$ symmetry.

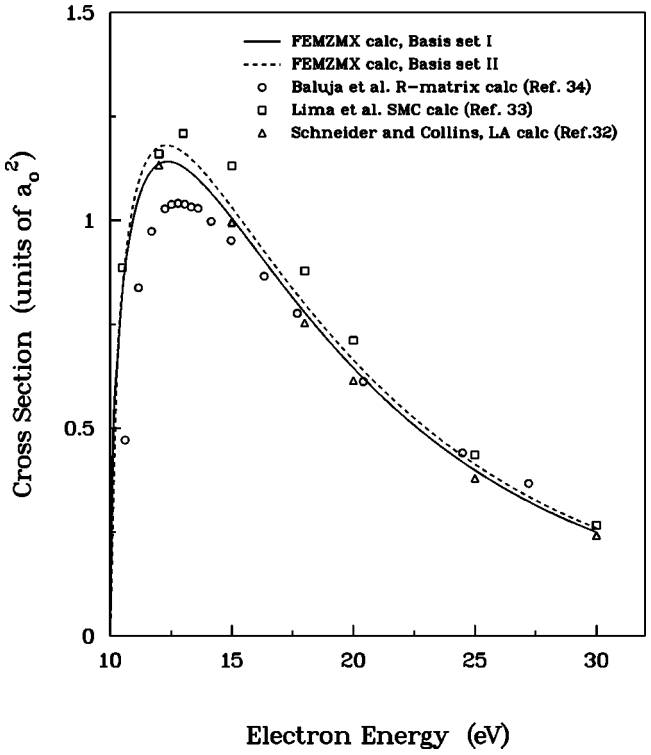

FIG. 2. Electron-impact excitation cross sections for the $X\,^1\Sigma_g^+ \rightarrow b\,^3\Sigma_u^+$ transition of H_2. $^2\Sigma_u^+$ symmetry.

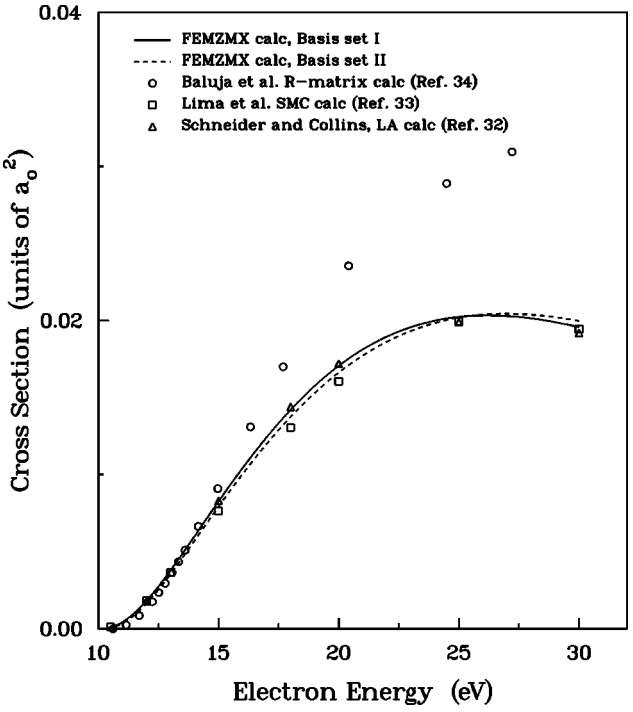

FIG. 3. Electron-impact excitation cross sections for the $X\,^1\Sigma_g^+ \rightarrow b\,^3\Sigma_u^+$ transition of H_2. $^2\Pi_{ux}$ symmetry.

for the difference is the closed-channel polarization functions included in *R*-matrix calculations. Thus the *R*-matrix treatment of the two-channel problem is different from the present approach as well as the SMC and LA studies. We have carried out *Z*-matrix calculations including closed-channel polarization functions, and found pseudoresonances at the high-energy end of the cross-section curve. As expected, the pseudoresonances are basis set dependent. The fact that no pseudoresonance was reported in Ref. [34] probably is due to the particular target basis used. In view of the presence of the pseudoresonances, we choose to present the results without polarization functions. It should also be pointed out that, comparing with Fig. 2 in Ref. [34], which includes their $^2\Sigma_g^+$ and $^2\Sigma_u^+$ partial cross sections without polarization, we find the remaining discrepancies with the *R*-matrix result are still larger than our discrepancies with the SMC and LA results.

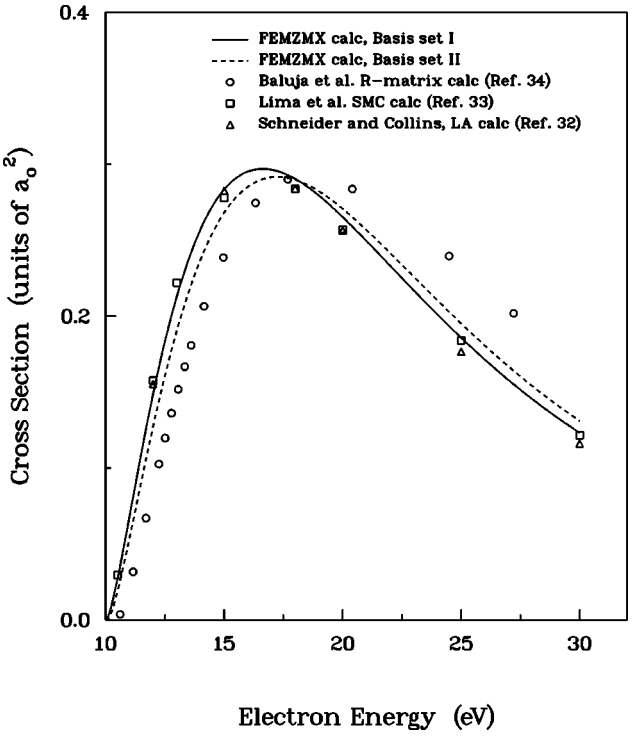

FIG. 4. Electron-impact excitation cross sections for the $X\,^1\Sigma_g^+ \rightarrow b\,^3\Sigma_u^+$ transition of H_2. $^2\Pi_{gx}$ symmetry.

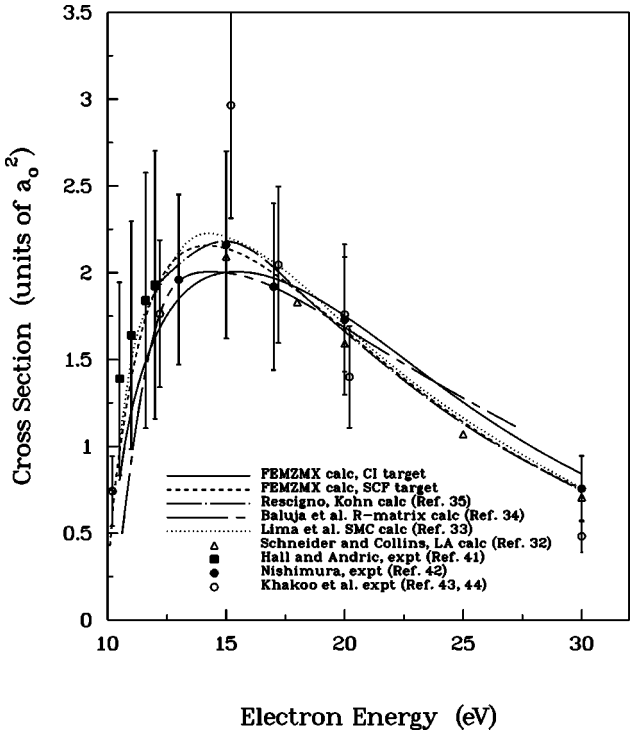

FIG. 5. Total electron-impact excitation cross sections for the $X\,^1\Sigma_g^+ \rightarrow b\,^+\Sigma_u^+$ transition of H_2.

Figure 5 presents the total excitation cross section for the $X\,^1\Sigma_g^+ \rightarrow b\,^3\Sigma_u^+$ transition calculated at R_e (≈ 1.4 a.u.) using the larger basis and with both CI and SCF targets. Other theoretical results are also presented. Besides the SMC, LA, and *R*-matrix calculations cited above, Rescigno and Schneider [35] reported a complex Kohn calculation over a range of internuclear distances using a two-configuration CI function for the ground state and an IVO function for the excited state. Their result at $R = 1.4$ a.u. is included in the figure. Also, Tennyson and co-workers carried out seven-state *R*-matrix calculations of electronic excitations of H_2 at $R = 1.4$ [36,37] and over a range of *R* values [38,39] using full CI target wave functions and a complete set of closed-channel function. Due to the use of closed-channel functions, their result is not directly comparable to ours, and thus not included in the figure.

As in the case of partial cross sections, the *Z* matrix, SMC, and LA results using SCF target functions are in close agreement. The *Z*-matrix result using full CI target functions stands somewhat apart, being lower than the SCF result in the low-energy region, and becomes higher at the high-energy end. Perhaps not surprisingly, the complex Kohn cross sections fall into the group using SCF targets. A major source for the difference between using CI and SCF targets

comes from the shift of the excitation threshold. The incomplete correlation treatment of the target in the complex Kohn calculation gives an excitation threshold at $R=1.4$ a.u. of 10.11 eV, a value closer to our SCF threshold (10.0076 eV) than the CI value of 10.6478 eV. Thus it is not surprising that their CI result is close to the SCF result. Note that the *R*-matrix result using SCF target stands somewhat apart from other results. In fact, they are closer to the *Z*-matrix result using full CI rather than SCF targets.

While fixed-nuclei calculations cannot be directly compared with experiment, it may still be useful to present experimental data as a qualitative guide. For this purpose, Fig. 5 also presents the experimental cross sections of Hall and Andrić [40], Nishimura [41], and Khakoo and co-workers [42,43]. Note that a calculation including nuclear motion, such as that of Stibbe and Tennyson [44] would have sampled the portion of vibrational wave function with $R>R_e$. Because the *b*-state energy rapidly decreases with increasing R near R_e, the experimental threshold will be lower than the threshold value determined at R_e. Since the SCF threshold is lower than the CI threshold, this fortuitously causes the fixed-nuclei cross sections determined using SCF target functions to agree better with experiment near threshold than the CI result. In spite of these qualifications, all calculated cross sections fall within the experimental uncertainties.

V. DISCUSSIONS

The *Z*-matrix method, implemented using a mixed finite-element and Gaussian basis, has been found to provide a robust computational method for *e*-molecule collisions. The power of variational stability in the *Z*-matrix formulation is demonstrated by the internal agreement of the eigenphase sums calculated using different sets of parameters.

The *Z*-matrix formulation can readily be extended to a two-dimensional case. This will include nonadiabatic treatment of nuclear motion, such as vibrational excitation or dissociation of a diatomic molecule by electron impact, the $(e,2e)$ problem for a molecular target, and electron collision of a Rydberg molecule. Such a two-dimensional code is under development. Because both sectorial calculations and the use of finite elements are well suited for massively parallel computers, the high demand for computing resources in a two-dimensional *Z*-matrix calculation may be alleviated by the use of massive parallelization.

ACKNOWLEDGMENTS

W.M.H. would like to thank Professor Janine Shertzer for her helpful advice in the use of finite elements. She is also grateful to Professor Jonathan Tennyson and Dr. Barry Schneider for their useful comments.

[1] E. P. Wigner and L. Eisenbud, Phys. Rev. A **72**, 29 (1947).
[2] K. L. Baluja, P. G. Burke, and L. A. Morgan, Comput. Phys. Commun. **27**, 299 (1982).
[3] J. L. Jackson, Phys. Rev. **83**, 301 (1951).
[4] R. S. Oberoi and R. K. Nesbet, Phys. Rev. A **8**, 215 (1973); **9**, 2804 (1974).
[5] D. E. Manolopoulos and R. E. Wyatt, Chem. Phys. Lett. **152**, 23 (1988); **159**, 123 (1989); D. E. Manolopoulos, M. D'Mello, and R. E. Wyatt, J. Chem. Phys. **91**, 6096 (1989).
[6] D. Brown and J. C. Light, J. Chem. Phys. **101**, 3723 (1994).
[7] P. G. Burke, A. Hibbert, and W. D. Robb, J. Phys. B **4**, 1153 (1971); P. G. Burke and M. J. Seaton, Methods Comput. Phys. **10**, 1 (1971); P. G. Burke and W. D. Robb, Adv. At. Mol. Phys. **11**, 143 (1975).
[8] P. G. Burke, I. Mackey, and I. Shimamura, J. Phys. B **10**, 2497 (1977); C. J. Noble, P. G. Burke, and S. Salvini, *ibid.* **15**, 3779 (1979).
[9] B. I. Schneider, Chem. Phys. Lett. **2**, 237 (1975); Phys. Rev. A **11**, 1957 (1975).
[10] B. I. Schneider, M. Le Dourneuf, and P. G. Burke, J. Phys. B **12**, L365 (1979).
[11] P. J. A. Buttle, Phys. Rev. **160**, 719 (1967).
[12] R. K. Nesbet, C. J. Noble, L. A. Morgan, and C. A. Weatherford, J. Phys. B **17**, L891 (1984); R. K. Nesbet, C. J. Noble, and L. A. Morgan, Phys. Rev. A **34**, 2798 (1986).
[13] C. J. Gillan, J. Tennyson, and P. G. Burke, in *Computational Methods for Electron-Molecule Collisions*, edited by W. M. Huo and F. A. Gianturco (Plenum, New York, 1995), Chap. 10, p. 239.
[14] K. Pfingst, B. M. Nestmann, and S. D. Peyerimhoff, in *Computational Methods for Electron-Molecule Collisions* (Ref. [13]), p. 293.
[15] L. A. Morgan, C. J. Gillan, J. Tennyson, and X. Chen, J. Phys. B **30**, 4087 (1997).
[16] J. Botero and J. Shertzer, Phys. Rev. A **46**, R1155 (1992); J. Shertzer and J. Botero, *ibid.* **49**, 3673 (1994).
[17] F. Abdolsalami, M. Abdolsalami, and P. Gomez, Phys. Rev. A **50**, 360 (1994).
[18] C. A. Weatherford, M. Dong, and B. C. Saha, Int. J. Quantum Chem. **65**, 591 (1997).
[19] K. J. Bathe and E. Wilson, *Numerical Methods in Finite Element Analysis* (Prentice-Hall, Englewood Cliffs, NJ, 1976); L. R. Ram-Mohan, S. Saigal, D. Dossa, and J. Shertzer, Comput. Phys. **4**, 50 (1990).
[20] P. M. Prenter, *Splines and Variational Methods* (Wiley, New York, 1975); see also Ref. [19].
[21] A different approach is used by the convergent close-coupling method and the intermediate-energy *R* matrix with pseudostates, two recent formulations employing a full set of target functions including pseudostates in the close-coupling expansion. See I. Bray and A. T. Stelbovics, Phys. Rev. A **46**, 6995 (1992); K. Bartschat, E. T. Hudson, M. P. Scott, P. G. Burke, and V. M. Burke, J. Phys. B **29**, 115 (1996).
[22] T. N. Rescigno, C. W. McCurdy, A. E. Orel, and B. H. Lengsfield III, in *Computational Methods for Electron-Molecule Collisions* (Ref. [13]), p. 1.
[23] W. M. Huo (unpublished).
[24] SWEDEN is an electronic structure program written by J. Almlöf, C. W. Bauschlicher, M. R. A. Blomberg, D. P. Chong, A. Heiberg, S. R. Langhoff, P.-A. Malmqvist, A. P. Rendell,

B. O. Roos, P. E. M. Siegbahn, and P. R. Taylor.
[25] I. Shavitt, in *Methods of Electronic Structure Theory*, edited by H. F. Schaefer III (Plenum, New York, 1977) Chap. 6, p. 189.
[26] A. E. Orel, T. N. Rescigno, and B. H. Lengsfield III, Phys. Rev. A **44**, 4328 (1991).
[27] J. Tennyson, J. Phys. B **29**, 1817 (1996).
[28] N. F. Mott and H. S. W. Massey, *The Theory of Atomic Collisions* (Oxford University Press, Oxford, 1965), p. 530.
[29] T. H. Dunning, J. Chem. Phys. **90**, 1007 (1989); R. A. Kendall, T. H. Dunning, and R. J. Harrison, *ibid.* **96**, 6796 (1992).
[30] W. Kolos and L. Wolniewicz, J. Chem. Phys. **43**, 2429 (1965).
[31] W. A. Goddard III and W. J. Hunt, Chem. Phys. Lett. **24**, 464 (1974).
[32] B. I. Schneider and L. A. Collins, J. Phys. B **18**, L857 (1985).
[33] M. A. P. Lima, T. L. Gibson, W. M. Huo, and V. McKoy, J. Phys. B **18**, L865 (1985).
[34] K. L. Baluja, C. J. Noble, and J. Tennyson, J. Phys. B **18**, L851 (1985).
[35] T. N. Rescigno and B. I. Schneider, J. Phys. B **21**, L691 (1988).
[36] S. E. Branchett and J. Tennyson, Phys. Rev. Lett. **64**, 2889 (1990).
[37] S. E. Branchett, J. Tennyson, and L. A. Morgan, J. Phys. B **23**, 4625 (1990).
[38] D. T. Stibbe and J. Tennyson, Phys. Rev. Lett. **79**, 4116 (1997).
[39] D. T. Stibbe and J. Tennyson, J. Phys. B **31**, 815 (1998).
[40] R. I. Hall and L. Andrić, J. Phys. B **17**, 3815 (1984).
[41] H. Nishimura, J. Phys. Soc. Jpn. **55**, 3031 (1986).
[42] M. A. Khakoo, S. Trajmar, R. McAdams, and T. W. Shyn, Phys. Rev. A **35**, 2832 (1987).
[43] M. A. Khakoo and J. Segura, J. Phys. B **27**, 2355 (1994).
[44] D. T. Stibbe and J. Tennyson, New J. Phys. **1**, 2.1 (1998).